Design and Optimization of Segmented PM Consequent Pole Hybrid Excited Flux Switching Machine for EV/HEV Application

Wasiq Ullah, Faisal Khan, *Member, IEEE*, and Muhammad Umair

***Abstract*— Hybrid Excited Flux Switching Machines (HEFSMs) unique feature of high torque density (T_{den}) of Permanent Magnet (PM) machines and flux regulation capability of wound field excitation machines. Due to aforesaid unique features, stator active HEFSMs are preferred for EV/HEV applications. In this paper a new Segmented PM Consequent Pole HE-FSM (SPMCPHEFSM) with flux bridge is proposed for EV/HEV. The developed SPMCPHEFSM exhibits improved flux modulation and flux regulation capability at reduced PM usage (suppressed PM volume by 46.52% and PM cost by 46.48%) and eliminating stator leakage flux. First, SPMCPHEFSM is geometric optimized (GO) for investigating influence of leading design with key performance indicators such as flux linkage (Φ_{pp}), average torque (T_{avg}), cogging torque (T_{cog}), T_{den}, average power (P_{avg}) and power density (P_{den}) and then proceeded optimized model to structure modification for optimal stator design and position of field excitation coils (FEC). Comprehensive performance analysis reveals that the developed SPMCPHEFSM show improved Φ_{pp} maximum up to 9.11%, improved T_{avg} maximum up to 23.63%, truncate T_{cog} up to 18.9% whereas T_{den} and P_{den} are boost up to 23.55% and 89.72% respectively.**

***Index Terms*— Electric Vehicle, Hybrid Electric Vehicle, Consequent Pole, Finite Element Analysis, Optimization, Segmented PM**

I. Introduction

FLUX Switching Machines (FSMs) are examples of stator active brushless AC machine in which all the excitations sources (Permanent Magnets, field winding slot and Armature winding slots) resides on stator leaving passive rotor made of iron only. Due to double salient structure and simple robust rotor structure, FSMs exhibits sinusoidal flux linkage and back emf therefore, applicable for brushless AC applications. FSMs are simple structure with key features of improved heat dissipation, relaxed thermal management of excitation source and mechanically robust structure. The design, structure and class of FSMs varies based on presence of the excitation sources.

Based on excitation source, FSMs are classified in to three major class i.e. Permanent Magnet (PM) excited, field excited and Hybrid excited (PM and field excited) [1]. The three major class of the FSMs becomes Permanent Magnet FSMs (PM-FSMs), Field Excited FSMs (FE-FSMs) and Hybrid Excited FSMs (HE-FSMs). Among three major FSMs categories, FE-FSM provide better flux controllability however offer low torque and power densities. PM-FSMs provides higher torque density however utilizes high PM volume and suffer from uncontrol and constant PM flux which causes issues of voltage regulation [2]. HE-FSM provide adjustable magnetic field and better flux controllability due exitance of both PM and field excitation winding in stator without effecting output characteristics. This flux controllability i.e. flux-weakening and flux enhancing capability are achieved with the help of field excitation current makes HE-FSM competent candidates for variable speed applications [3, 4] especially in Electric Vehicles (EVs) and Hybrid Electric Vehicles (HEVs). In addition, flux controllability provides ratio of the PM flux and field excitation winding flux which results investigation of wide constant power speed range [5, 6]. Based on the aforesaid merits of HE-FSM, this paper solely focuses on detail investigation regarding structure variations as well torque and power capability of HE-FSM for EV and HEV applications.

A comprehensive overview of HE-FSM for EV and HEVs are discussed in [7] whereas various classification of HE-FSM for EV/HEV based on position of PM and field excitation coils (FEC) reported in literature are listed in Fig. 1. Author in [8] mentioned series and parallel HE-FSM however in series HE-FSM PM permeability is same as air resulting higher excitation circuit reluctance. Flux controllability of HE-FSMs are improved utilizing iron ring at the outermost with concentrated field winding at the stator yoke in [9] whereas concept of iron flux bridge is presented in [10]. However narrow flux bridges easily saturated under loaded condition and heat up machine parts. The resultant heat causes PM demagnetization which degraded electromagnetic performance and its operation. Author in [11] developed HE-FSMs for hybrid vehicle from the existing PM-FSMs topologies by reducing the PM volume to reserve the space for field winding however flux regulation solely depend on PM length in axial direction. Moreover, the reverse current applied to field excitation winding causes PM demagnetization of the adjacent PMs. The flux regulation theories in HE-FSMs is investigated in [12]. Detailed analysis reveals that partial PM flux short circuited which results in decrease of the torque density. The torque production is improved in PM memory machines with novel flux regulation methodology utilizing High Coercive force (HCF) and low coercive force (LCF) PM. However, flux regulation range of memory machines are limited since flux is controllable in the maximum and minimum HCF and LCF magnetization state [13]-[15].

Manuscript was submitted for review on 23, May, 2020.
This work receives no funding source yet.
Wasiq Ullah, Faisal Khan and Muhammad Umair are with the Department of Electrical and Computer Engineering, COMSATS University Islamabad, Abbottabad Campus, 22060, Pakistan. E-mails: (wasiqullah014@gmail.com, faisalkhan@cuiatd.edu.pk, muhammadumair1221@gmail.com)
Digital Object Identifier 10.30941/CESTEMS.2020.00026

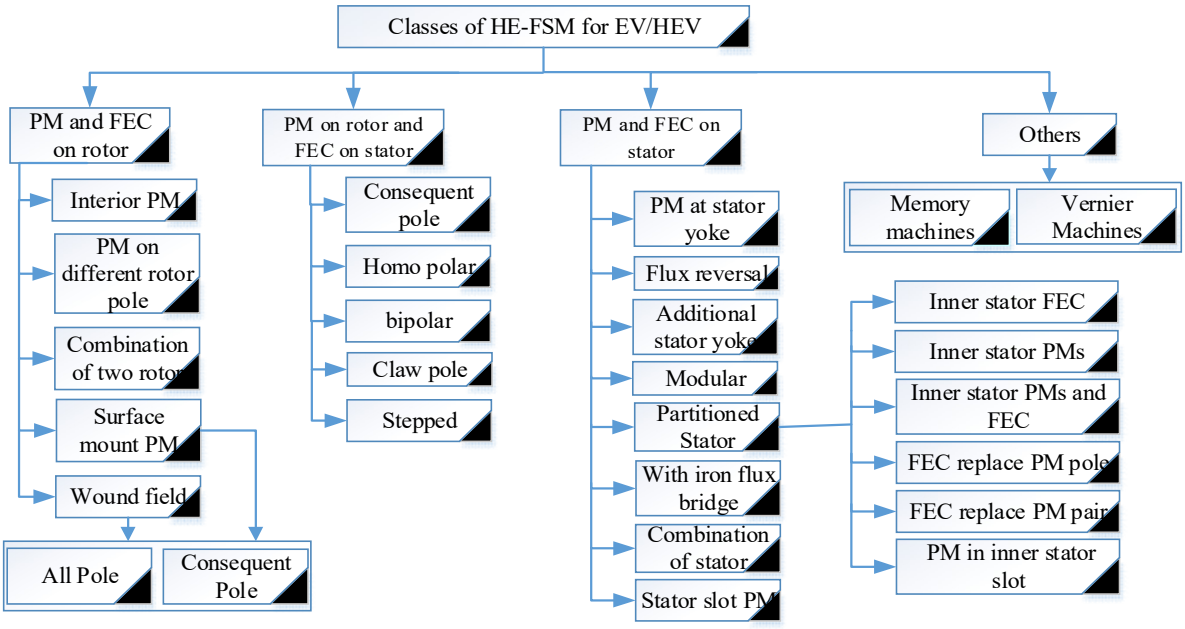

Fig. 1. Classification of HE-FSMs based on position of PM and FEC for EV/HEV application.

Author in [3] investigated HE-FSM for EV and HEV applications with E-core stator and excitation winding on fault-tolerant teeth however since armature and field winding generates flux with reverse polarities, the flux regulation capability is limited which further effect wide speed operation range. In order to overcomes the flux regulation capability, author in [16] introduces dual-stator HE-FSMs to accommodate separate stator for armature field winding and field excitation winding however, in this case the design becomes highly complex due to iron-piece rotor sandwich between both stators. Moreover, the machine volume increases and due to iron-piece rotor it suffers from mechanical constraint and are not considered favorable for high speed applications.

Authors in [17]-[20] introduced surface-mounted synchronous machines with both PM and FEC coils lie on rotor surface attaching FEC to all PM poles and consequent pole configuration however, flux path of the FEC coils passes over PM causes significant reluctance and limited flux regulation capability. The additional flux path to FEC coil is provided in IPM through iron bridge and suppressed risk of irreversible demagnetization, however due to narrow bridge saturation, the flux regulation capability still remains limited. To overcome the aforesaid demerits, author in [21, 22] directly combine rotor PM machine and rotor wound field machine where both PM field and wound field are attached to same shaft. In this design flux path of PM and FEC are inherently separated through parallel hybridization to achieve higher flux regulation capability. However, since wound field are at rotor, brushes and slip rings are required which increases maintenance cost and reduces system reliability due to mechanical contact. The requirement of brushes and slip rings are eliminated in brushless HE topologies in [23]-[28] however machine topology and drive circuit become complicated. Moreover, spatial confliction of PM and DC coils limit torque density and flux regulation capability.

In order to overcome the aforesaid demerits in various HE-FSMs designs regarding flux controllability, flux regulation capability, position of armature and field winding, torque and power densities, this paper introduces a new topology of Segmented PM (SPM) Consequent Pole HE-FSM (SPMCPHEFSM) for EV and HEV as shown in Fig. 2. The developed model utilized SPM with Circumferential Magnetization PMs (CM-PMs) and Radial Magnetization PMs (RM-PMs) to reduce the overall PM volume and introduces flux bridges to improve the flux modulation phenomena. SPMCPHEFSM is constructed and investigated regarding for flux controllability, flux regulation capability, working principle and proceed to optimization, geometric modification for optimal stator structure, position of armature and field winding and comparison of various SPMCPHEFSM topologies. It is worth mentioning that SPMCPHEFSM is extension of the previously studies of author regarding SPM Consequent Pole FSM (SPMCPFSM) with only PM excitation [29]-[31] which were proposed on [32] to reduce PM volume and curtailed flux circulation within flux bridge and flux barrier. In comparison of the aforesaid models, the proposed model greatly helps in PM volume reduction by 46.52% and suppression of circulating flux in stator core. Initially, in SPMCPFSM design, armature winding is halved and allocate it to field excitation winding and later on geometric modification is performed for optimum position and stator structure.

Main contributions of this paper include designing of a new SPMCPHEFSM for EV and HEV application at 46.52% reduced PM volume that suppress the overall PM cost by 46.48 and enhancing the flux modulation, flux controllability and power density. Furthermore, Geometric Optimization (GO) is investigated for enhancing electromagnetic performance and to achieving optimum design parameters. The optimized SPMCPHEFSM is updated for various stator structure and optimum position of field excitation winding. Comprehensive

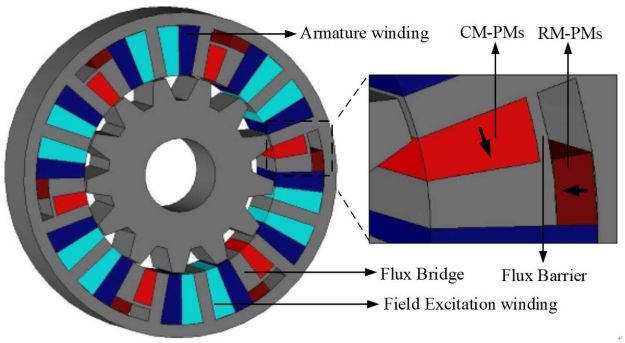

Fig. 2. Proposed SPMCPHEFSM topology.

performance analysis reveals that the developed SPMCPHEFSM show improved Φ_{pp} maximum up to 9.11%, enhanced T_{avg} maximum up to 23.63% suppressed T_{cog} up to 18.9%, whereas T_{den} and P_{den} up to 23.55% and 89.72 respectively.

In the following, SPMCPHEFSM topology and flux regulation capability are shown in section II, section III discusses geometric optimization, afterward, optimized model is proceeded to structural modification and comparison in section IV. Finally, some conclusions are drawn in section V.

II. SPMCPHEFSM Topology and Flux Regulation Capability

A. SPMCPHEFSM Topology

Design parameters of proposed SPMCPHEFSM is listed in Table I and indicated in Fig 3. Cross sectional view of SPMCPHEFSM shows that each armature winding coils are concentrated between segmented PMs with different magnetization pattern i.e. CM-PMS and RM-PMs which are enclosed between flux bridge, flux barrier and stator teeth. The flux bridge not only act as 2nd pole of the PMs but also provide magnetic path for flux distribution and linkage that ultimately helps in enhancing flux modulation phenomena and reducing the total PM usage.

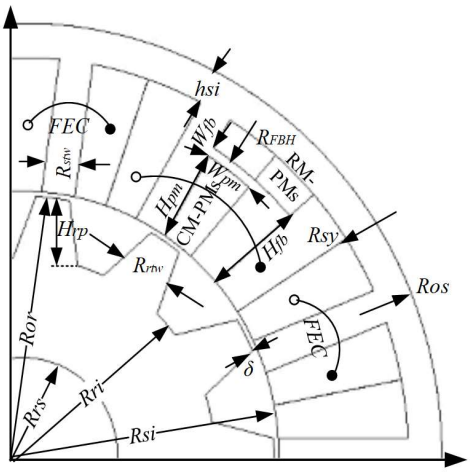

Fig. 3. Illustration of design dimension for SPMCPHEFSM.

SPMCPHEFSM enclosed PMs in h-shaped stator teeth to eliminate stator leakages flux going across the stator thus, converting leakage flux to flux linkage. It is worth mentioning that in SPMCPHEFSM, flux distribution and linkage though airgap occurs from stator yoke as well as flux bridge (as shown in Fig. 4). This superposition of flux improves flux modulation phenomena to superimpose each other by through flux bridge and barriers and results higher magnetic flux density which ultimately improve torque/power production capability. This dual modulation phenomena in SPMCPHEFSM improves overall performance and results higher torque/power density and better electromagnetic performance.

TABLE I
MAJOR GEOMETRIC PARAMETER OF SPMCPHEFSM

Symbol	Parameter (unit)	Value (mm)
R_{os}	Outer radius of stator	45
R_{sy}	Inner radius of stator yoke	41.4
R_{FBH}	Radius of flux bridge	37
h_{si}	Stator back iron height	3.6
R_{si}	Stator inner radius	27.5
R_{ri}	Rotor inner radius	20.4
R_{or}	Rotor outer radius	27
R_{rtw}	Rotor tooth width	3.6
R_{stw}	Stator slot width	3.6
H_{pm}	CM-PM height	8.5
W_{pm}	CM-PM width	3.03
H_{fb}	Flux bridge height	9.5
W_{fb}	Flux bridge width	1.0
H_{rp}	Rotor pole height	6.6
L	Axial length	25
σ	Air gap length	0.5

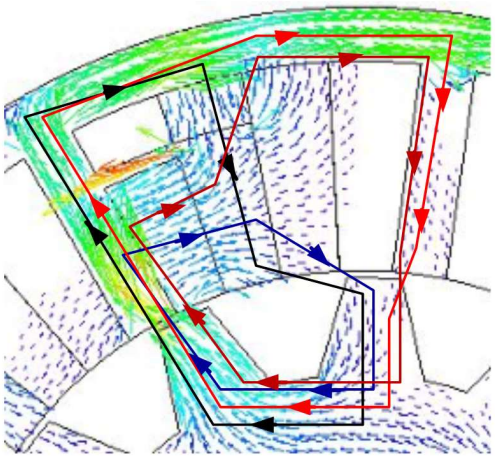

Fig. 4. Flux Modulation in SPMCPHEFSM.

B. Flux Regulation Capability

The flux controllability of the proposed SPMCPHEFSM mainly depend on the excitation current. The flux distribution under different excitation sources (only PM source and both PM and FEC) is shown in Fig. 5 whereas flux enhancing and flux weakening condition are as shown in Fig. 6. It can be clearly seen that the flux linked to armature windings are contribution of both PM flux and FEC flux. Analysis reveals that the flux linkage can be easily controlled by injecting field current with different polarities.

The flux enhancing and flux weakening capability is further investigated under various field excitation current density i.e. $J_e = 0, \pm5, \pm10, \pm15\ (A/mm^2)$ is shown in Fig. 7. Analysis unveils that under flux enhancing operation mode ($J_e > 0$) air-gap flux density enhanced resulting increase in the flux linkage with the increase in positive excitation current whereas under flux weakening operation mode ($J_e < 0$) air-gap flux density is

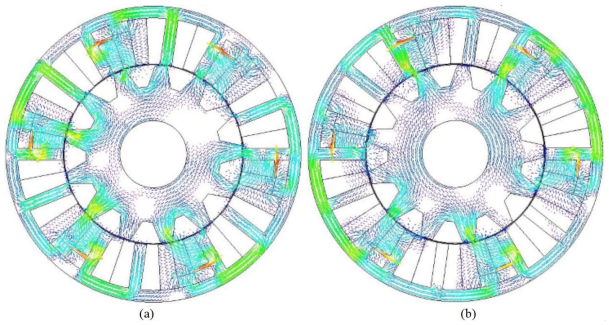

Fig. 5. Flux distribution with (a) PM excitation and (b) PM and FEC.

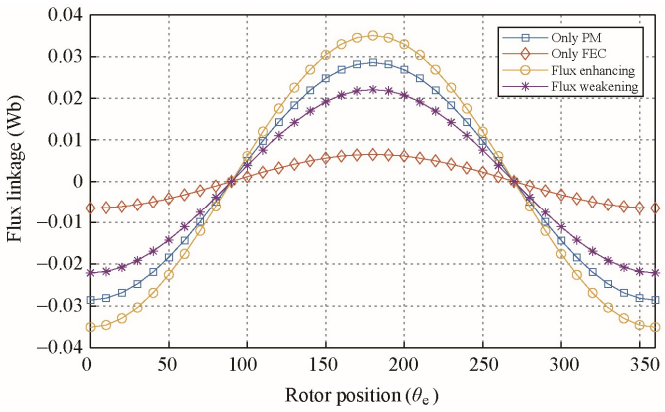

Fig. 6. Flux linkage under different excitation source.

deteriorated resulting decrease in the flux linkage with the increase in the negative excitation current. Furthermore, it can be clearly seen that under various identical field excitation current and different polarities, the flux linkage is symmetrical and sinusoidal. Overall, this verify flux enhancing and flux weakening capability of SPMCPHEFSM and confirm that flux regulation capability solely depends on excitation current.

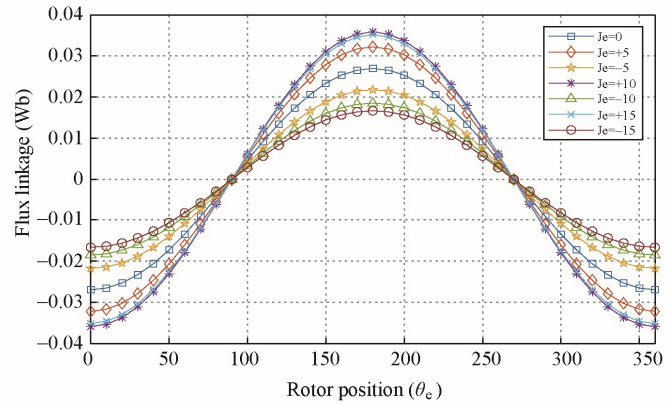

Fig. 7. Variation of the flux linkage under flux enhancing and weakening operation mode before optimization.

III. GEOMETRIC OPTIMIZATION

Electromagnetic performance of the developed SPMCPHEFSM is enhanced utilizing Geometric Optimization (GO) with key performance indicator such as flux linkage (Φ_{pp}), flux linkage Harmonic (Φ_{THD}), average torque (T_{av}), cogging torque (T_{cog}), torque ripples (T_{rip}), torque density (T_{den}), average power (P_{avg}), and power density (P_{den}). Overall, GO is implemented in multiple steps with detailed flow as shown in Fig. 8. Key performance indicators are calculated as

$$\Phi_{THD} = \frac{\sqrt{\sum_{i=2}^{N} U_i^2}}{U_1} \tag{1}$$

$$T_{rip} = T_{max} - T_{min} \tag{2}$$

$$T_{den} = \frac{T_{avg}}{V_{PM}} \tag{3}$$

$$P_{den} = \frac{P_{avg}}{W_{PM}} \tag{4}$$

Where as U_i is ith harmonic terms, U_1 is fundamental harmonic terms, T_{max} is maximum torque peak, T_{min} is minimum torque peak, V_{PM} is PM volume and W_{PM} is PM weight. Note that V_{PM} and W_{PM} for proposed SPMCPHEFSM is $8091.25\ mm^3 \approx 8.09125\text{x}10^{-6}\ \text{m}^3$ and 0.061 kg, respectively.

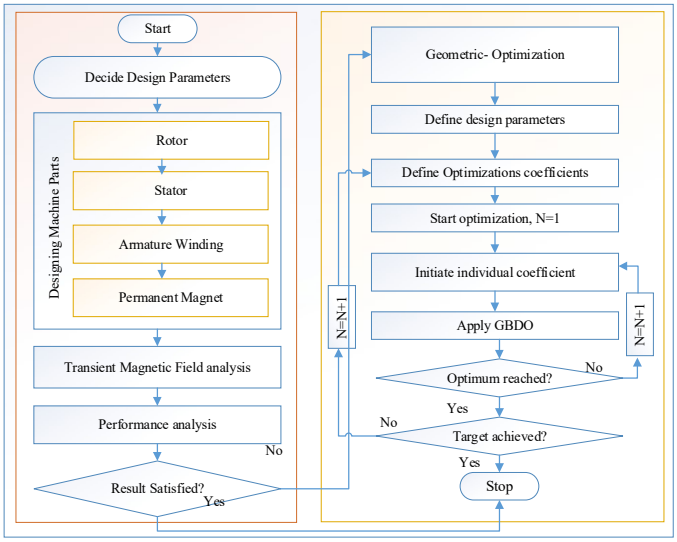

Fig. 8. Flow chart of geometric Optimization.

In this process, initial design parameters of SPMCPHEFSM based on their sensitivity are opted for optimization. GO is implemented such that most sensitive design parameter is optimized first and then proceed to next level with previous stage optimum design. In this process, sequentially GO optimize leading design parameters of rotor as well as stator. GO is opted based on objective function, constraint and boundary condition as

$$\begin{cases} Objective\ function \\ \max\ (T_{avg}, T_{den}, P_{avg}, T_{den})\ and \\ \min\ (T_{cog}, T_{rip}) \end{cases} \tag{5}$$

$$\begin{cases} Constraint \\ T_{avg} > 2.5\ Nm,\ \ T_{cog} < 2\ Nm,\ \Phi_{THD} \le 2\% \\ T_{rip} < 2.5\ Nm, T_{den} > 310\ kNm/m^3 \\ P_{den} > 12.45\ kW/\text{kg and}\ P_{avg} > 760\ \text{W} \end{cases} \tag{6}$$

$$\begin{cases} Boundry\ condition \\ 0.55 \le \beta_s \le 0.65 \\ 2.47 \le R_{rtw} \le 7.74 \\ 5.1 \le H_{pm} \le 10.1 \\ 2.5 \le W_{pm} \le 5.0 \\ 5.1 \le H_{fb} \le 10.1 \\ 0 \le W_{fb} \le 1.0 \end{cases} \tag{7}$$

Note that during GO, electrical loading (number of turns and applied current), magnetic loading (PM volume), slot area, stack length and air gap length are kept constant. Influence of GO in various optimization steps on different design parameters are discussed in the proceeding sub-sections.

A. β_s Optimization

β_s is the ratio of R_{si} and R_{so}. In this optimization step, the influence of the stator length is investigated by varying R_{si}. The maximum and minimum values of β_s is restricted to $h_{si}/2$ and $2 * h_{si}$ to avoid magnetic saturation and ensure uniform magnetic field distribution. β_s shows major influences in variation of T_{avg}, T_{cog}, T_{den} and T_{rip}. Performance analysis with varying β_s is shown in Fig. 9 and listed in Table II.

Performance analysis of initial developed SPMCPHEFSM, and β_s optimizations (term as SPMCPHEFSM-1) reveals that T_{cog} is reduced by 23.5%, improve T_{avg} by 2.85%, suppressed T_{rip} by 22.08%, enhance T_{den} by 2.84%. Note that initially β_s was 0.61 and in this stage, it is updated to 0.56.

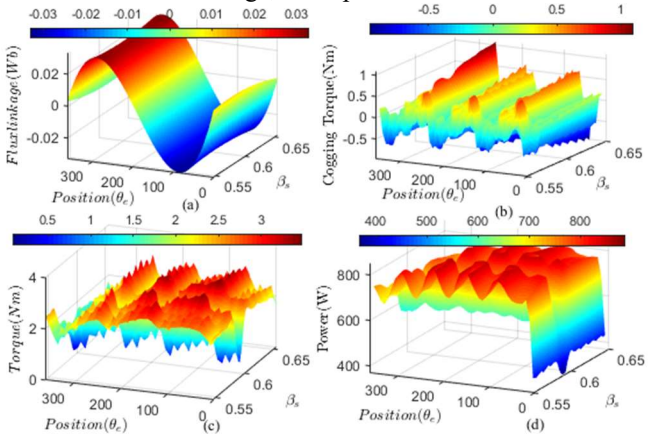

Fig. 9. Effect of β_s optimization on (a) Flux linkage (b) Cogging Torque (c) Instantaneous torque (d) Power.

TABLE. II
PERFORMANCE ANALYSIS WITH β_s OPTIMIZATION

Performance indicator (unit)	SPMCPHEFSM	SPMCPHEFSM-1
Φ_{pp} (Wb)	0.0702896	0.066853
Φ_{THD} (%)	1.2694068	1.5262796
T_{cog} (Nm)	1.9126697	1.463334
T_{avg} (Nm)	2.5092076	2.580643
T_{rip} (Nm)	2.7329393	2.1293237
T_{den} (kNm/m^3)	310.11372	318.94244
P_{avg} (W)	762.7645	764.25831
P_{den} (kW/kg)	12.50433	12.52882

B. R_{rtw} Optimization

This step analyzed influence of R_{rtw} on electromagnetic performance. R_{rtw} is varied for optimal point between 2.47 mm and 7.74-mm. Detailed performance analysis with the variation of R_{rtw} is shown in Fig. 10 and listed in Table III. It can be clearly seen that R_{rtw} show major influence in variation of the of T_{avg}, Φ_{THD}, T_{rip}, P_{avg} and T_{den}.

Performance analysis of SPMCPHEFSM-1, and R_{rtw} optimizations (term as SPMCPHEFSM-2) reveals that T_{avg} is improved by 1.4%, suppressed Φ_{THD} by 16.4%, enhance T_{den} by 1.37% at the cost of 2.7% increase in T_{cog}. Note that initially R_{rtw} was 7 mm and in this phase, it is updated to 4.86 mm.

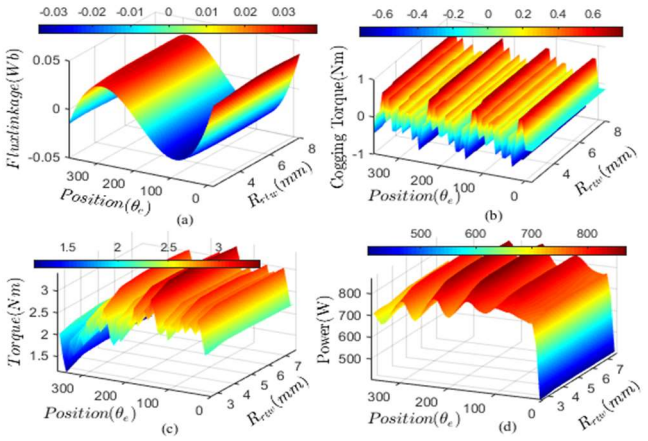

Fig. 10. Effect of R_{rtw} optimization on (a) Flux linkage (b) Cogging Torque (c) Instantaneous torque (d) Power.

TABLE. III
ELECTROMAGNETIC PERFORMANCE ANALYSIS WITH R_{rtw} OPTIMIZATION

Performance indicator (unit)	SPMCPHEFSM-1	SPMCPHEFSM-2
Φ_{pp} (Wb)	0.066853	0.0679052
Φ_{THD} (%)	1.5262796	1.2267575
T_{cog} (Nm)	1.463334	1.5007552
T_{avg} (Nm)	2.580643	2.6167771
T_{rip} (Nm)	2.1293237	2.1775138
T_{den} (kNm/m^3)	318.94244	323.40826
P_{avg} (W)	764.25831	769.13881
P_{den} (kW/kg)	12.52882	12.60883

C. H_{pm} Optimization

Proposed SPMCPHEFSM design utilized SPM with CM-PMs and RM-PMs enclosed inside flux bridge and flux barrier. In this step, H_{pm} of the CM-PMs is investigated. It is worth mentioning that while varying H_{pm} of the CM-PMs, the respective height of the RM-PMs is varied to fix the PM volume. It is also worth mentioning that H_{pm} is same as height of the flux bridge.

In this phase, CM-PMs H_{pm} is varied between 8 mm to 12 mm and their corresponding electromagnetic performance are shown in Fig. 11 and listed in Table IV. Performance analysis of SPMCPHEFSM-2, and H_{pm} optimizations (term as SPMCPHEFSM-3) unveil that H_{pm} exhibit slight variation on electromagnetic performance. Note that initially H_{pm} was 10 mm and in this stage, it is updated to 11 mm. It is worth mentioning that H_{pm} is the same as H_{fb}.

TABLE. IV
ELECTROMAGNETIC PERFORMANCE ANALYSIS WITH H_{pm} OPTIMIZATION

Performance indicator (unit)	SPMCPHEFSM-2	SPMCPHEFSM-3
Φ_{pp} (Wb)	0.0679052	0.068713
Φ_{THD} (%)	1.2267575	1.2451442
T_{cog} (Nm)	1.5007552	1.4640959
T_{avg} (Nm)	2.6167771	2.6116359
T_{rip} (Nm)	2.1775138	2.1455895
T_{den} (kNm/m^3)	323.40826	322.77286
P_{avg} (W)	769.13881	773.55154
P_{den} (kW/kg)	12.60883	12.681173

D. W_{fb} Optimization

Structure of proposed SPMCPHEFSM enclosed CM-PMs and RM-PMs in flux barrier which provide physical isolation of

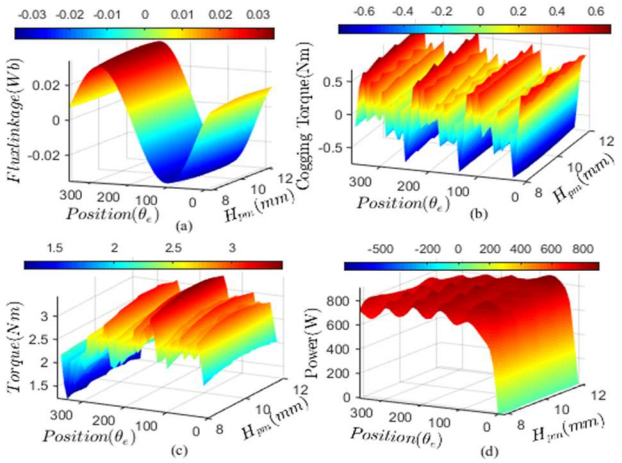

Fig. 11. Effect of H_{pm} optimization on (a) Flux linkage (b) Cogging Torque (c) Instantaneous torque (d) Power.

both PMs and provide alternate path to working harmonics to enhanced flux modulation phenomena however it causes flux circulation which degrade electromagnetic performances. In this optimization phase, W_{fb} is optimized so that ensure least possible flux circulation and flux leakage.

Detailed electromagnetic performance with variation of W_{fb} is shown in Fig. 12 and listed in Table V. Performance analysis of SPMCPHEFSM-3, and W_{fb} optimizations (term as SPMCPHEFSM-4) reveals that Φ_{pp} is enhanced by 3.05%, enhance T_{avg}, T_{den} by 1.37% at the cost of 3.7% increase in Φ_{THD}. Note that initially W_{fb} was 1 mm and in this point, it is updated to 0 mm such that the flux barrier is removed.

TABLE. V
ELECTROMAGNETIC PERFORMANCE ANALYSIS WITH W_{fb} OPTIMIZATION

Performance indicator (unit)	SPMCPHEFSM-3	SPMCPHEFSM-4
Φ_{pp} (Wb)	0.068713	0.0694038
Φ_{THD} (%)	1.2451442	1.2871991
T_{cog} (Nm)	1.4640959	1.5844472
T_{avg} (Nm)	2.6116359	2.6877762
T_{rip} (Nm)	2.1455895	2.2986872
T_{den} (kNm/m^3)	322.77286	332.18306
P_{avg} (W)	773.55154	779.19051
P_{den} (kW/kg)	12.681173	12.77361

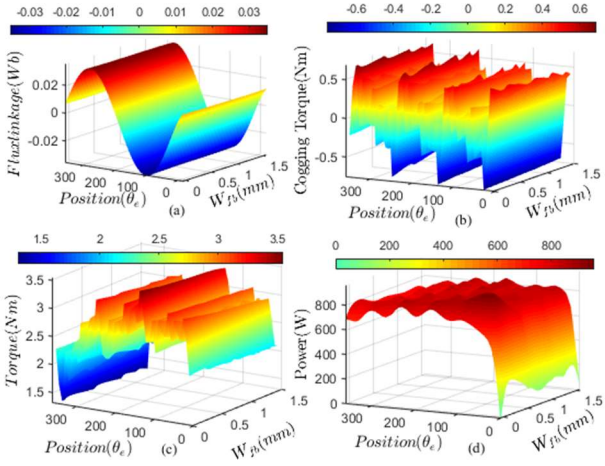

Fig. 12. Effect of W_{fb} optimization on (a) Flux linkage (b) Cogging Torque (c) Instantaneous torque (d) Power.

E. W_{pm} Optimization

In final phase of GO, W_{pm} of CM-PM is optimized to ensure least possible slotting effects. In this stage, W_{pm} of CM-PM is varied between 3.9 mm to 1.71 mm. In order to keep the PM volume constant, span of the RM-PMs is varied to ensure fix magnetic loading. W_{pm} shows major influences in variation of T_{avg}, P_{avg}, T_{den} and P_{den}. Performance analysis with variation of W_{pm} is shown in Fig. 13 and listed in Table VI.

Electromagnetic performance comparison of SPMCPHEFSM-4, and W_{pm} optimizations (term as SPMCPHEFSM-5) reveals that T_{avg} is enhance by 2.89%, whereas T_{den} is improved by 2.65% at the cost of 1.2% increase in T_{avg}. Note that initially W_{pm} was 3.03 mm and in this stage, it is updated to 2.59 mm.

TABLE. VI
ELECTROMAGNETIC PERFORMANCE ANALYSIS WITH W_{pm} OPTIMIZATION

Performance indicator (unit)	SPMCPHEFSM-4	SPMCPHEFSM-5
Φ_{pp} (Wb)	0.0694038	0.0695326
Φ_{THD} (%)	1.2871991	2.0101235
T_{cog} (Nm)	1.5844472	1.6718445
T_{avg} (Nm)	2.6877762	2.7577553
T_{rip} (Nm)	2.2986872	2.2515639
T_{den} (kNm/m^3)	332.18306	340.8318
P_{avg} (W)	779.19051	781.33921
P_{den} (kW/kg)	12.77361	12.80883

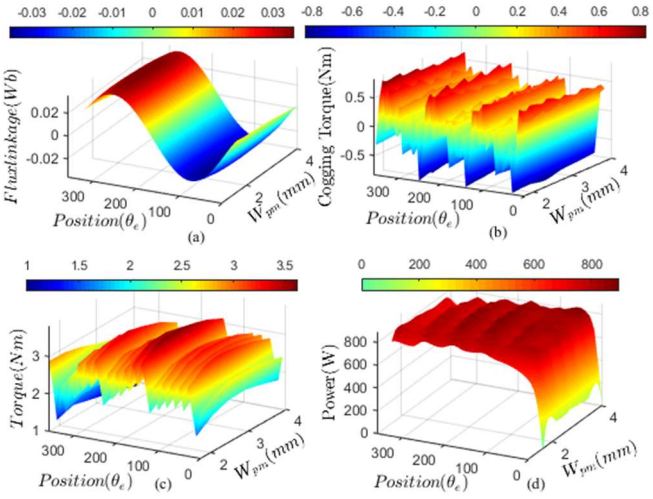

Fig. 13. Effect of W_{pm} optimization on (a) Flux linkage (b) Cogging Torque (c) Instantaneous torque (d) Power.

The overall GO process sequentially optimized rotor and stator. Table VII shows initial and optimized design parameters of SPMCPHEFSM, Fig. 14 shows cross sectional view of initial and optimized design whereas electromagnetic performance of initial and optimized designed are compared in Table VIII.

TABLE. VII
INITIAL AND OPTIMIZED DESIGN PARAMETERS OF SPMCPHEFSM

Parameter	Initial value	Optimized value
β_s	0.61	0.58
H_{pm}	10	11
W_{pm}	3.05	2.59
W_{fb}	1	0
R_{rtw}	7	4.86

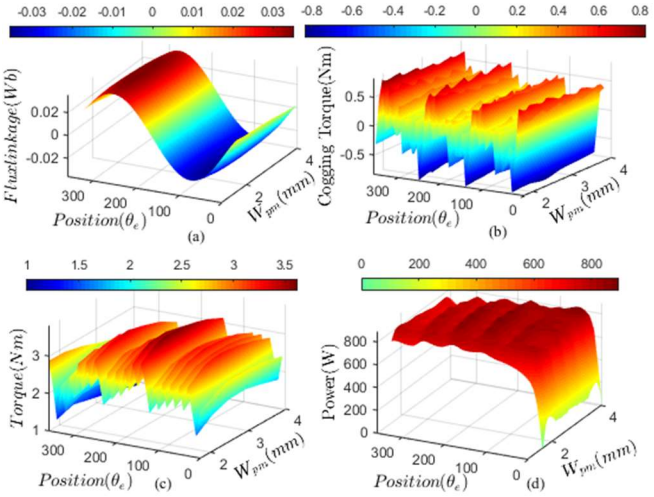

Fig. 13. Effect of W_{pm} optimization on (a) Flux linkage (b) Cogging Torque (c) Instantaneous torque (d) Power.

TABLE. VIII
ELECTROMAGNETIC PERFORMANCE ANALYSIS OF INITIAL AND OPTIMIZED SPMCPHEFSM

Performance indicator (unit)	Initial design	Optimized design (Model-1)
Φ_{pp} (Wb)	0.0702896	0.0695326
Φ_{THD} (%)	1.2694068	2.0101235
T_{cog} (Nm)	1.9126697	1.6718445
T_{avg} (Nm)	2.5092076	2.7577553
T_{rip} (Nm)	2.7329393	2.2515639
T_{den} (kNm/m^3)	310.11372	340.8318
P_{avg} (W)	762.7645	781.33921
P_{den} (kW/kg)	12.50433	12.80883

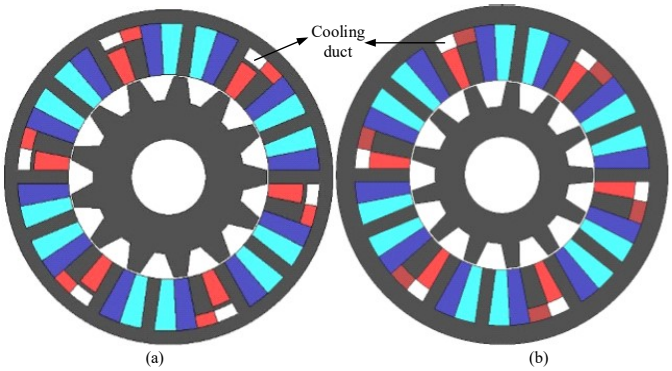

Fig. 14. Cross sectional view of (a) Initial design (b) Optimized design (Model-1).

Detailed quantitative electromagnetic performance analysis of initial and optimized SPMCPHEFSM reveal that T_{cog} is supressed by 12.59%, T_{avg} is improved by 9.9%, truncated T_{rip} by 17.61%, increased P_{avg} by 2.43%, increased T_{den} by 9.9% and P_{den} by 2.43% at the cost of 1.06% increase in Φ_{pp}.

The optimized model is further investigated for flux weakening and flux enhancing capability. Fig. 15 shows flux regulation capability of the optimized model. In comparison with flux regulation capability before optimization (as shown in Fig. 5) it can be clearly seen that when applied filed excitation current density i.e. $J_e = \pm 15\ A/mm^2$, before optimization, 30.37% flux enhancing capability and 38.14% flux weakening capability is achieved whereas after optimization, 13.35% flux enhancing capability and 32.89% flux weakening capability is achieved. It is the evidence that after optimization flux regulation capability is slightly reduces.

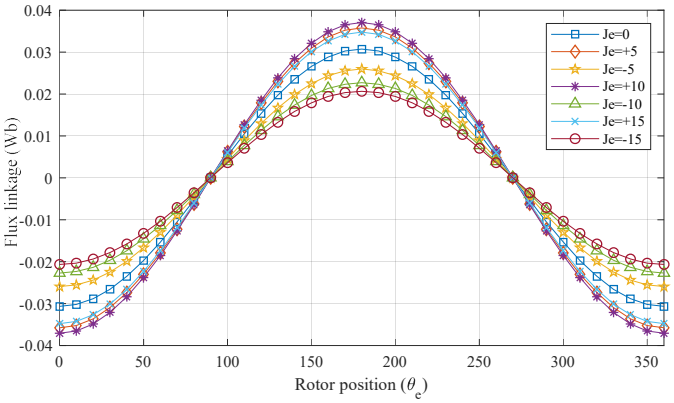

Fig. 15. Variation of the flux linkage under flux enhancing and weakening operation mode after optimization.

IV. STRUCTURAL MODIFICATION AND COMPARISON

In this section, the optimized model (term as Model-1) is investigated for alternate position of the FEC and modified stator structure for improved electromagnetic performance. In this regard, initially position of the FEC are shifted to reserved space between PMs and the updated model (term as Model-2) is shown in Fig. 16(a). Furthermore, the model is reduced to E-Core and C-core as shown in Fig. 16(b) and Fig. 16(c) which are term as Model-3 and Model-4 respectively. Detailed quantitative electromagnetic performance of aforesaid topologies is listed in Table IX.

Detailed performance of the all models (Model-1 to Model-4) are shown in Fig. 17 to Fig. 20. Comparison of Model-1 with Model-2 shows that, structural modification in Model-2 exhibits 9.11% higher Φ_{pp}, 8.1% however reduces P_{den} by 47.29% and offer lower T_{cog}, T_{avg}, T_{den}, P_{avg}. In addition, comparison with Model-3 reveals that Model-3 exhibits 23.63% higher T_{avg}, 23.55% higher T_{den} by 13.34% and lower P_{den} by 11.87%. Moreover, comparison with Model-4 reveals that Model-4 exhibits 13.45% higher T_{avg}, 13.18% and 5.49% lower T_{den}.

To sum up, it is noted that proposed SPMCPHEFSM show improved Φ_{pp} maximum up to 9.11%, enhanced T_{avg} maximum up to 23.63%, suppressed T_{cog} up to 18.9%, whereas improves T_{den} up to 23.55% and P_{den} up to 89.72%.

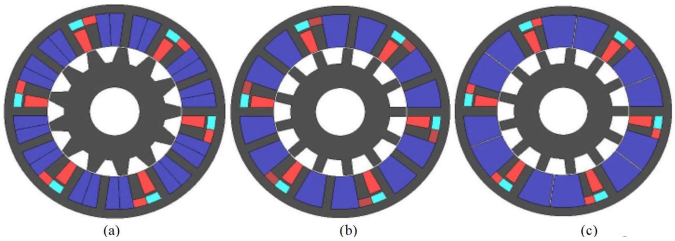

Fig. 16. Cross sectional view of SPMCPHEFSM topologies (a) Model-2 (b) Model-3 and (c) Model-4.

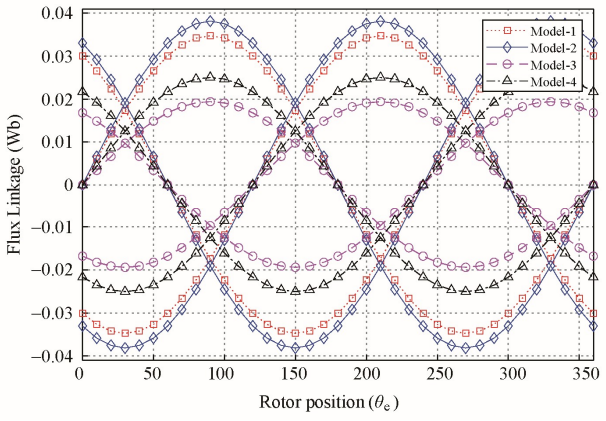

Fig. 17. Comparison of flux linkage.

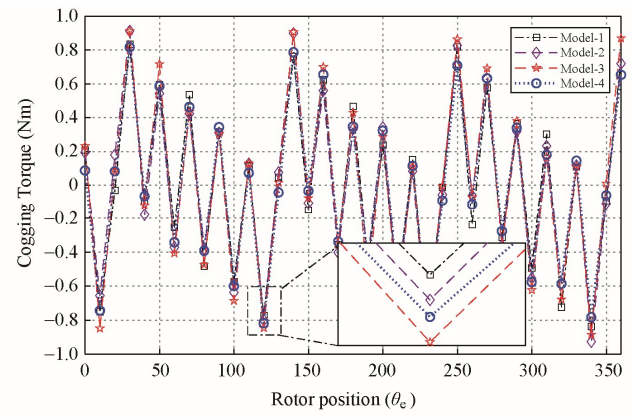

Fig. 18. Cogging torque comparison.

TABLE. IX
QUANTITATIVE PERFORMANCE ANALYSIS OF VARIOUS SPMCPHEFSM TOPOLOGIES

Performance (unit)	Model-2	Model-3	Model-4
Φ_{pp} (Wb)	0.07587	0.05460	0.06683
Φ_{THD} (%)	5.82401	24.7840	23.4950
T_{cog} (Nm)	1.83841	1.79742	1.63534
T_{avg} (Nm)	2.52567	3.40733	3.12143
T_{rip} (Nm)	2.97348	2.49208	2.2522
T_{den} (kNm/m^3)	312.149	421.113	385.779
P_{avg} (W)	411.824	688.563	738.442
P_{den} (kW/kg)	6.751213	11.28791	12.1056

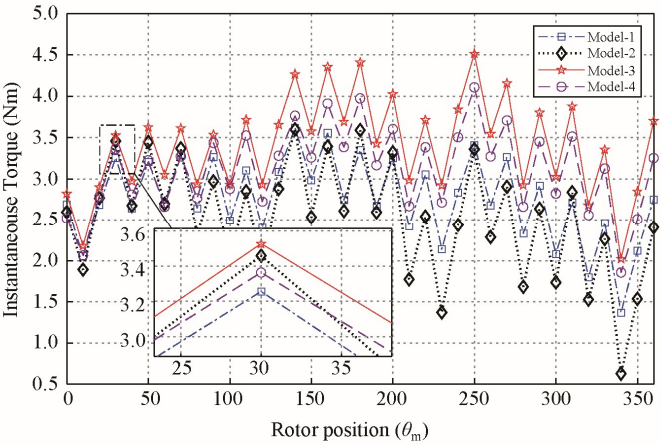

Fig. 19. Instantaneous torque of all models.

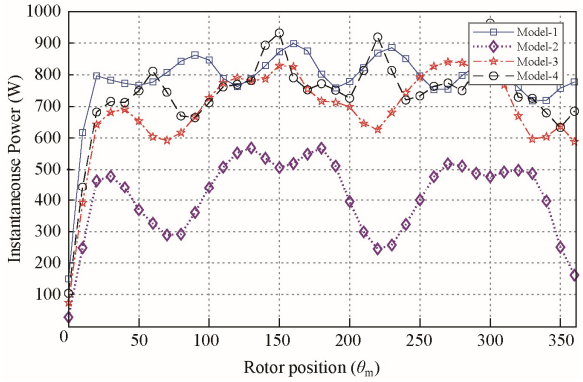

Fig. 20. Power capability of all models.

V. CONCLUSION

This paper proposed and investigates a new SPMCPHEFSM with flux bridge for EV/HEV application. Proposed SPMCPHEFSM exhibits enhanced flux modulation and flux regulation capability at reduced PM usage utilizing CM-PMs and RM-PMs that suppressed PM volume by 46.52% and PM cost by 46.48% and eliminating stator leakage flux. Furthermore, influence of leading design parameters is investigated utilizing geometric optimization and proceeded to structure modification for optimal stator design and position of excitation winding. Analysis reveals that proposed SPMCPHEFSM show improved Φ_{pp} maximum up to 9.11%, improved T_{avg} maximum up to 23.63%, truncate T_{cog} up to 18.9% whereas T_{den} and P_{den} are boost up to 23.55%.

REFERENCES

[1] Ullah, Wasiq; Khan, Faisal; Umair, Muhammad, "Sub-Domain Modelling and Multi-Variable Optimization of Partitioned PM Consequent Pole Flux Switching Machines", *IET Electric Power Applications*, vol. 14, no. 8, pp. 1360-1369, 2020.

[2] K. T. Chau, C. C. Chan and C. Liu, "Overview of Permanent-Magnet Brushless Drives for Electric and Hybrid Electric Vehicles," *in IEEE Transactions on Industrial Electronics,* vol. 55, no. 6, pp. 2246-2257, June 2008

[3] J. T. Chen, Z. Q. Zhu, S. Iwasaki, and R. P. Deodhar, "A novel hybrid excited switched-flux brushless AC machine for EV/HEV applications*," IEEE Trans. Veh. Technol.,* vol. 60, no. 4, pp. 1365–1373, May 2011.

[4] B. Gaussens, E. Hoang, M. Lecrivain, P. Manfe, and M. Gabsi, "A hybrid-excited flux-switching machine for high-speed DC-alternator applications*," IEEE Trans. Ind. Electron.,* vol. 61, no. 6, pp. 2976–2989, Jun. 2014.

[5] Y. Amara, L. Vido, M. Gabsi, E. Hoang, A. H. B. Ahmed, and M. Lecrivain, "Hybrid excitation synchronous machines: Energy efficient solution for vehicles propulsion," *IEEE Trans. Veh. Technol.,* vol. 58, no. 5, pp. 2137–2149, Jun. 2009.

[6] F. G. Capponi, G. Borocci, G. De Donato, and F. Caricchi, "Flux regulation strategies for hybrid excitation synchronous machines," *IEEE Trans. Ind. Appl.,* vol. 51, no. 5, pp. 3838–3847, Sep./Oct. 2015.

[7] Z. Q. Zhu and S. Cai, "Hybrid excited permanent magnet machines for electric and hybrid electric vehicles," *in CES Transactions on Electrical Machines and Systems,* vol. 3, no. 3, pp. 233-247, Sept. 2019

[8] X. Zhu, Z. Xiang, C. Zhang, L. Quan, Y. Du, and W. Gu, "Co-reduction of torque ripple for outer rotor flux-switching PM motor using systematic multi-level design and control schemes," *IEEE Trans. Ind. Electron.,* vol. 64, no. 2, pp. 1102-1112, Feb. 2017.

[9] E. Hoang, M. Lecrivain, and M. Gabsi, "A new structure of a switching flux synchronous polyphased machine with hybrid excitation," *in Proc. Eur. Conf. Power Electron. Appl. (EPE)*, Sep. 2007, pp. 1–8.

[10] R. L. Owen, Z. Q. Zhu, G. W. Jewell, "Hybrid excited flux-switching permanent-magnet machines with iron flux bridges," *IEEE Trans. Magn.,* vol. 46, no. 6, pp. 1726-1729, 2010.

[11] W. Hua, M. Cheng and G. Zhang, "A novel hybrid excitation flux-switching motor for hybrid vehicles", *IEEE Trans. Magn.,* vol. 45, no. 10, pp. 4728-4731, Dec. 2009.
[12] W. Hua, G. Zhang, and M. Cheng, "Flux-regulation theories and principles of hybrid-excited flux-switching machines," *IEEE Trans. Ind. Electron.,* vol. 62, no. 9, pp. 5359–5369, Sep. 2015.
[13] X. Zhu, Z. Xiang, L. Quan, W. Wu, and Y. Du, "Multimode optimization design methodology for a flux-controllable stator permanent magnet memory motor considering driving cycles," *IEEE Trans. Ind. Electron.,* vol. 65, no. 7, pp. 5353–5366, Jul. 2018.
[14] H. Yang et al., "Hybrid-excited switched-flux hybrid magnet memory machines," *IEEE Trans. Magn.,* vol. 52, no. 6, pp. 1–15, Jun. 2016.
[15] F. Li, K. T. Chau, C. Liu, J. Z. Jiang, and W. Y. Wang, "Design and analysis of magnet proportioning for dual-memory machines," *IEEE Trans. Appl. Supercond.,* vol. 22, no. 3, Jun. 2012.
[16] H. Hua and Z. Q. Zhu, "Novel Hybrid-Excited Switched-Flux Machine Having Separate Field Winding Stator," *in IEEE Transactions on Magnetics,* vol. 52, no. 7, pp. 1-4, July 2016
[17] G. Henneberger, J. R. Hadji-Minaglou, and R. C. Ciorba, "Design and test of permanent magnet synchronous motor with auxiliary excitation winding for electric vehicle application," *in Proc. Eur. Power Electron. Symp.,* Oct. 1994, pp. 645–649.
[18] D. Fodorean, A. Djerdir, I. Viorel and A. Miraoui, "A double excited synchronous machine for direct drive application—design and prototype tests," *IEEE Trans. Energy Convers.,* vol. 22, no. 3, pp. 656-665, Sept. 2007.
[19] N. Lin, D. Wang, Y. Shen and K. Wei, "Investigation on hybrid ratio between PM and current excitation sources for high-speed synchronous generator," *in Proc. 2014 17th International Conference on Electrical Machines and Systems (ICEMS), Hangzhou,* 2014, pp. 505-508.
[20] A. D. Akemakou and S. K. Phounsombat, "Electrical machine with double excitation, especially a motor vehicle alternator," *U.S. Patent* 6 147 429, Nov. 14, 2000.
[21] C. Syverson, and W. Francis, "Hybrid alternator", US Patent 5747909 B1/5 may 1998.
[22] N. Naoe and T. Fukami, "Trial production of a hybrid excitation type synchronous machine," *in Proc. IEMDC 2001. IEEE International Electric Machines and Drives Conference (Cat. No.01EX485),* Cambridge, MA, USA, 2001, pp. 545-547.
[23] Q. Ali, S. Atiq, T. A. Lipo, and B. I. Kwon, "PM assisted, brushless wound rotor synchronous machine," *J. Magn.,* vol. 21, no. 3, pp. 399–404, Nov. 2016.
[24] A. Hussain, S. Atiq and B. Kwon, "Consequent-pole hybrid brushless wound-rotor synchronous machine," *IEEE Trans. Magn.,* vol. 54, no. 11, pp. 1-5, Nov. 2018.
[25] F. Yao, Q. An, X. Gao, L. Sun and T. A. Lipo, "Principle of operation and performance of a synchronous machine employing a new harmonic excitation scheme," *IEEE Trans. Ind. Appl.,* vol. 51, no. 5, pp. 3890-3898, Sept.-Oct. 2015.
[26] G. Jawad, Q. Ali, T. A. Lipo and B. Kwon, "Novel brushless wound rotor synchronous machine with zero-sequence third-harmonic field excitation," *IEEE Trans. Magn.,* vol. 52, no. 7, pp. 1-4, July 2016.
[27] Q. Ali, T. A. Lipo and B. Kwon, "Design and analysis of a novel brushless wound rotor synchronous machine," *IEEE Trans. Magn.,* vol. 51, no. 11, pp. 1-4, Nov. 2015.
[28] A. Hussain and B.-I. Kwon, "A new brushless wound rotor synchronous machine using a special stator winding arrangement," *Elect. Eng.,* pp. 1–8, Nov. 2017.
[29] W. Ullah, F. Khan, N. Ullah, M. Umair, B. Khan and H. A. Khan, "Comparative Study Between C-Core/E-Core SFPMM with Consequent Pole SFPMM," *2019 International Symposium on Recent Advances in Electrical Engineering (RAEE),* Islamabad, Pakistan, 2019, pp. 1-6.
[30] W. Ullah, F. Khan, E. Sulaiman, M. Umair, N. Ullah and B. Khan, "Influence of Various Rotor Pole on Electromagnetic Performance of Consequent Pole Switched Flux Permanent Magnet Machine," *2019 International Conference on Electrical, Communication, and Computer Engineering (ICECCE), Swat, Pakistan,* 2019, pp. 1-6.
[31] Ullah, Wasiq; Khan, Faisal; Sulaiman, Erwan; Umair, Muhammad; Ullah, Noman; Khan, Bakhtiar: 'Analytical validation of novel consequent pole E-core stator permanent magnet flux switching machine', *IET Electric Power Applications,* 2020, 14, (5), p. 789-796, DOI: 10.1049/iet-epa.2019.0257
[32] Y. Gao, D. Li, R. Qu, H. Fang, H. Ding and L. Jing, "Analysis of a Novel Consequent-Pole Flux Switching Permanent Magnet Machine with Flux Bridges in Stator Core," *in IEEE Transactions on Energy Conversion,* vol. 33, no. 4, pp. 2153-2162, Dec. 2018.

Wasiq Ullah is basically from Afghanistan and was born in District Peshawar, Khyber Pakhtunkhwa, Pakistan in 1995. He received his B.S. and master's degree degrees in electrical (power) engineering from COMSATS University Islamabad (Abbottabad Campus), Abbottabad, Pakistan in 2018 and 2020 respectively. He is currently working as a research associate in COMSATS University Islamabad (Abbottabad Campus), Abbottabad, Pakistan for analytical modelling of electric machines in electric machine design research lab.
His research interests include analytical modelling, design analysis and optimization of Permanent Magnet Flux Switching Machines, Linear Flux Switching Machines, Hybrid Excited Flux Switching Machines and segmented permanent magnet Consequent pole Flux Switching Machines for high speed brushless AC applications.

Faisal Khan was born in District Charsadda, Khyber Pakhtunkhwa, Pakistan in 1986. He received his B.S. degree in electronics engineering from COMSATS University Islamabad (Abbottabad Campus), Pakistan in 2009 and M.S. degree in electrical engineering from COMSATS University Islamabad (Abbottabad Campus), Pakistan in 2012. He received Ph.D. degree in electrical engineering from Universiti Tun Hussein Onn Malaysia, Malaysia in 2017.
From 2010 to 2012, he was a Lecturer at University of Engineering & Technology, Abbottabad, Pakistan. Since 2017, he has been Assistant Professor with the Electrical Engineering Department, COMSATS University Islamabad (Abbottabad Campus), Pakistan. He is author of more than seventy publications, one patent, and received multiple research awards. His research interests include design and analysis of flux-switching machines, synchronous machines, and DC machines

Muhammad Umair was born in District Peshawar, Khyber Pakhtunkhwa, Pakistan in 1995. He received his B.S. degrees in electrical (power) engineering from COMSATS University Islamabad (Abbottabad Campus), Abbottabad, Pakistan in 2018. He is currently perusing M.S degree in Electrical (Power) Engineering at COMSATS University Islamabad (Abbottabad Campus). His research interests include design, analysis, optimization and experimental validation of flux-switching machines.